Intracranial electroencephalography reveals effector-independent evidence accumulation dynamics in multiple human brain regions

Sabina Gherman[1], Noah Markowitz[1], Gelana Tostaeva[1], Elizabeth Espinal[1,2], Ashesh D. Mehta[1,3], Redmond G. O'Connell[4,5], Simon P. Kelly[6], Stephan Bickel[1,3,7]

Affiliations

[1]The Feinstein Institutes for Medical Research, Northwell Health, Manhasset, NY, United States

[2]Department of Psychological and Brain Sciences, Drexel University, Philadelphia, PA, United States

[3]Departments of Neurology and Neurosurgery, Zucker School of Medicine at Hofstra/Northwell, Hempstead, NY, United States

[4]Trinity College Institute of Neuroscience, Trinity College Dublin, Dublin, Ireland

[5]School of Psychology, Trinity College Dublin, Dublin, Ireland

[6]School of Electrical and Electronic Engineering and UCD Centre for Biomedical Engineering, University College Dublin, Dublin, Ireland

[7]Center for Biomedical Imaging and Neuromodulation, Nathan Kline Institute, Orangeburg, NY, United States

*Corresponding authors:

Sabina Gherman, agherman@northwell.edu

Stephan Bickel, sbickel@northwell.edu

Abstract

Neural representations of perceptual decision formation that are abstracted from specific motor requirements have previously been identified in humans using non-invasive electrophysiology, however, it is currently unclear where these originate in the brain. Here, we capitalized on the high spatiotemporal precision of intracranial EEG to localize such abstract decision signals. Participants undergoing invasive electrophysiological monitoring for epilepsy were asked to judge the direction of random-dot stimuli and respond either with a speeded button press (N=24), or vocally, after a randomized delay (N=12). We found a widely distributed motor-independent network of regions where high-frequency activity exhibited key characteristics consistent with evidence accumulation, including a gradual build-up that was modulated by the strength of the sensory evidence, and an amplitude that predicted subjects' choice accuracy and response time. Our findings offer a new view on the brain networks governing human decision making.

Introduction

A perceptual decision is the process of choosing among alternatives on the basis of sensory information, such as judging whether a traffic light is red or green. Such decisions are often tied to particular motor plans (e.g., braking if the light is red). This has motivated a large body of non-human primate neurophysiology work to characterize the neural correlates of perceptual decisions in regions of the brain involved in motor selection/planning, i.e., where activity is selective for the action used to express choice. Activity at these sites is consistent with a process of evidence accumulation, building gradually over time at a rate that is proportional with the strength of the sensory information, reaching a fixed threshold just before a response is made, and reliably predicting the animal's choice and response time[1–6].

In complex environments however, decisions about sensory events must often be made even when the appropriate movement is not known in advance, or when one is not required immediately. How such abstract (i.e., motor-independent) decisions are enabled by the brain remains unclear. In recent years, a concerted effort has been made to identify abstract decision signals in both human and non-human research. Single unit recordings in the non-human primate have uncovered signals that reflect choice-relevant categories independently of specific motor requirements, across parietal[7–9], prefrontal[10], and midbrain structures[11]. However, the limited spatial coverage in these studies precludes a comprehensive spatial mapping of the generators of similar signals. Meanwhile, human neuroimaging work has identified several regions across the prefrontal and parietal cortex where blood-oxygen-level-dependent (BOLD) signals correlate with the strength of sensory evidence irrespective of response modality[12–16]. However, the low temporal resolution of functional magnetic resonance imaging (MRI) precludes verification that these regions exhibit the expected evidence accumulation dynamics. Additionally, these studies differ in the assumptions they make regarding the expected BOLD profile of a region involved in decision making, and, consequently, there has been considerable variability across studies in the regions identified with this method.

Human electrophysiology has contributed high temporal precision and whole-brain analyses to the characterization of effector-independent decision dynamics. Several studies have been able to decode choice-selective activity for tasks involving stimulus presence/absence[17], intensity[18], or identity[19–21] judgments. However, an approach focused on choice selectivity could overlook areas of the brain where choice alternatives are represented by spatially intertwined or adjacent neuronal populations that are not separable with the relatively low spatial resolution of these techniques, as neuronal selectivity to choice and task properties can be highly heterogeneous even within small regions (e.g., LIP[22]).

Indeed, several scalp EEG studies have highlighted an abstract signature of evidence accumulation over centroparietal electrodes (the centro-parietal positivity or CPP) that undergoes a positive build-up during deliberation regardless of which alternative the cumulative evidence favors and which, therefore, would likely be missed by classifiers decoding choice-selective activity for two-alternative discriminations[23–26]. The CPP exhibits a unique combination of characteristics that can be leveraged in analyses designed to identify abstract evidence accumulation signals in intracranial recordings. These include a gradual buildup during deliberation, with a slope that scales with evidence strength[24,27] and predicts response time irrespective of evidence location[28] or sensory modality[23]. The CPP is also motor-independent, tracing the cumulative evidence when the stimulus-response mapping

is unknown at the time of evidence presentation[29] and even when no overt action is required at all[23]. An additional feature that distinguishes the CPP from the build-to-threshold signals observed in effector-selective areas is that its amplitude at the time of choice scales with accuracy and decreases as a function of reaction time, in contexts where choices must be reported within a strict deadline[25,27,30].

While CPP-like signals measured on the scalp appear to be in agreement with the existence of abstract representations of cumulative evidence, their generators in the brain are not currently known. Aside from offering a more detailed map of the neural architecture that supports decision making, establishing its generators would be a critical step toward understanding how decisions are represented in the brain. A scalp-recorded signal like the CPP may reflect the summation of activity from potentially multiple sources and thus obscure more complex spatiotemporal dynamics. Invasive recordings from human intracranial EEG could circumvent these limitations, as this method provides millimeter spatial precision, while preserving the temporal resolution of scalp EEG/MEG recordings[31]. Additionally, it offers broader spatial sampling compared to single-unit recordings.

Here, we recorded intracranial EEG (iEEG) in a large cohort (N=24) of pre-surgical epilepsy patients as they performed perceptual discrimination paradigms designed to allow characterization of evidence-dependent buildup signals in terms of their distinct temporal profile and selectivity for, or independence from, evidence location and motor response (Fig 1a). Subjects viewed two simultaneous random dot patches and were asked to report the direction of random-dot motion occurring in either one, with a speeded button press. To evaluate potential decision-related signals arising independently of motor requirements, a subset of participants (N=12) also performed a version of the task in which choices were reported vocally after a randomized delay. We identified multiple locations where high-frequency activity dynamics were consistent with abstract evidence accumulation, primarily distributed across prefrontal, parietal, inferior temporal, and insular regions. Specifically, we first selected electrodes that individually met criteria for consistency with scalp-measured evidence accumulation signals, namely evidence-dependent amplitude and independence from the responding effector (limb) or spatial location of the sensory evidence. We further demonstrated that activity amplitude at these sites correlated with behavioral speed and accuracy, and importantly, that they continued to exhibit evidence-dependent buildup dynamics under vocal responses. Our data provide an extensive mapping of abstract evidence accumulation dynamics across the human brain and a guide to future investigations into the neural substrate of abstract decisions.

Results

We recorded iEEG activity while subjects performed a two-stimulus motion discrimination task (Fig 1a). In each trial, two patches of incoherently moving dots appeared simultaneously on the left and right side of a fixation point, and following a random delay, one of them, selected at random, began to move coherently at either a high or low coherence level. The direction (upwards or downwards) of this motion was to be reported by the subject as quickly and as accurately as possible.

Manual response task

Behavior. In the speeded manual response version of the task (Fig. 1a), subjects were instructed to report their choice within a 2000 ms deadline by means of a button press with their left/right hand. As expected, we found that behavioral performance was strongly modulated by the strength of sensory evidence (i.e., motion coherence) across subjects, with stronger evidence leading to improved choice accuracy (Low coherence: M=79.83% correct, SD=7.69%; High coherence: M=90.06%, SD=5.73%; t(23)=6.98, p<0.001, *d*=1.48 , 95% CI: [0.84 2.11], paired-sample t-test, one-tailed) and shorter response times (Low coherence: M=1173 ms, SD=145 ms; High coherence: M=985 ms, SD=147 ms; t(23)=-12.2, p<0.001, *d*=-1.27, 95% CI: [-1.87 -0.65], paired-sample t-test, one-tailed) (Fig. 1b). Neither accuracy nor RT varied systematically with the direction of motion (upwards vs. downwards; Accuracy: t(23)=1.86; p=0.076, *d*=-0.43, 95% CI: [-1 0.13]; RT: t(23)=-0.004, p=0.997, *d*=0, 95% CI: [-0.56 0.56], paired-sample t-tests, two-tailed). The location of the sensory evidence did influence behavior, such that subjects tended to respond faster and more accurately when the stimulus was presented on the right side of the screen (Accuracy: t(23)=-2.49, p=0.021, *d*=0.54, 95% CI: [-0.03 1.11]; RT: t(23)=4.38, p<0.001, *d*=1.85, 95% CI: [1.17 2.52], paired-sample t-tests, two-tailed).

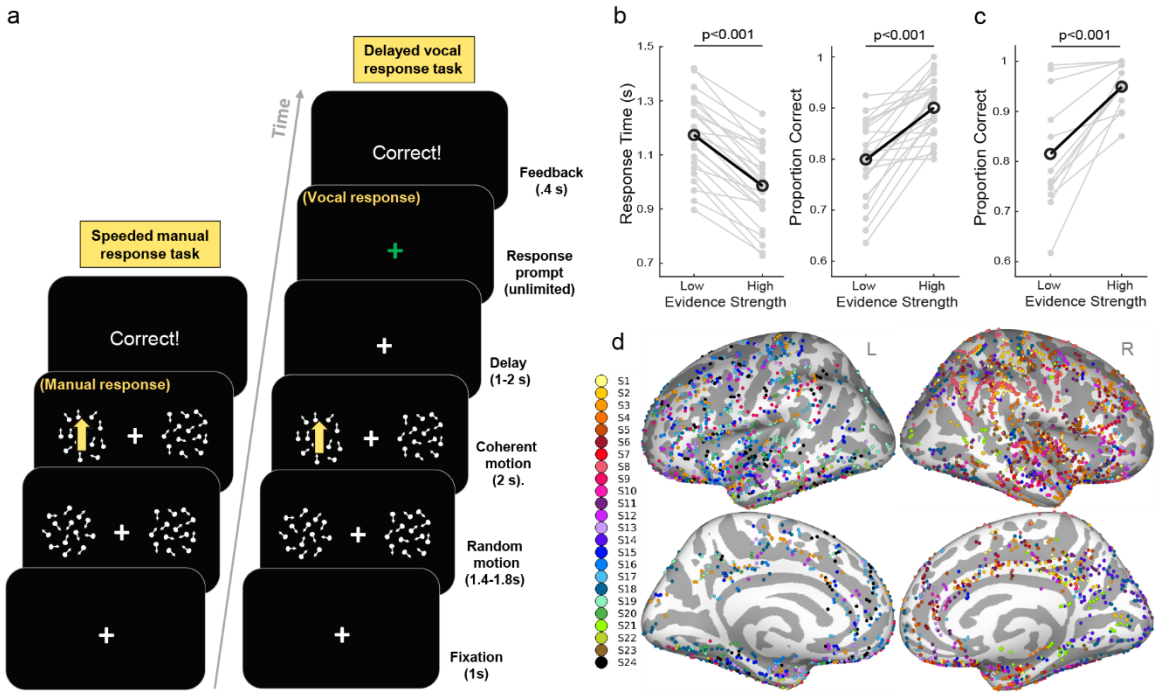

Figure 1. Experimental approach. a. Behavioral task design. On both tasks, subjects viewed two simultaneous patches of randomly moving dots, located laterally on each side of a fixation cross. After a random delay, motion on one (unpredictable) side became coherent, either upwards (90°) or downwards (270°), with motion coherence taking one of two possible values that approximately spanned perceptual threshold. In the manual response task (left panel), subjects reported the direction of the coherent motion as quickly and as accurately as possible, with a button click with their left/right hand, whose mapping to direction was counterbalanced across subjects. During the vocal response task (right panel), subjects were required to wait through the motion stimulus and an additional random delay (marked by a visual cue) before reporting their choice, and did so by verbally naming the direction of motion. Feedback was provided at the end of each trial for both versions of the task. **b.** Behavioral performance during the manual response task, as a function of motion coherence (left panel: response time; right panel: choice accuracy). Black data points represent averages across subjects. Gray data points represent individual subject data. **c.** Choice accuracy during the vocal response task as a function of motion coherence. P-values for **b** and **c** are based on one-tailed t-tests. **d.** Intracranial electrode coverage for the manual response task. Each color represents a subject. Electrodes have been projected onto the Freesurfer[59] average inflated brain (light gray: gyri; dark gray: sulci).

iEEG. We first identified contacts that exhibited task-responsive activity, measured as a significant ($p<0.01$, uncorrected) increase in high-frequency activity (HFA; 70-170 Hz) amplitude during the decision period (see Methods). Of the 3380 contacts included in the analysis (Fig. 1d), we found 1007 contacts that showed a significant HFA response following the transition from incoherent to coherent motion (Fig. 2a-c). These task responsive sites were distributed widely across the brain (Fig. 2a, c) and initial inspection of their activity indicated heterogeneity in time courses and alignment to evidence onset vs. response execution (for an example of two contacts with distinct alignment to the two events, see Fig. 2d). All subsequent analyses of the neural data were performed on the subset of contacts identified at this step.

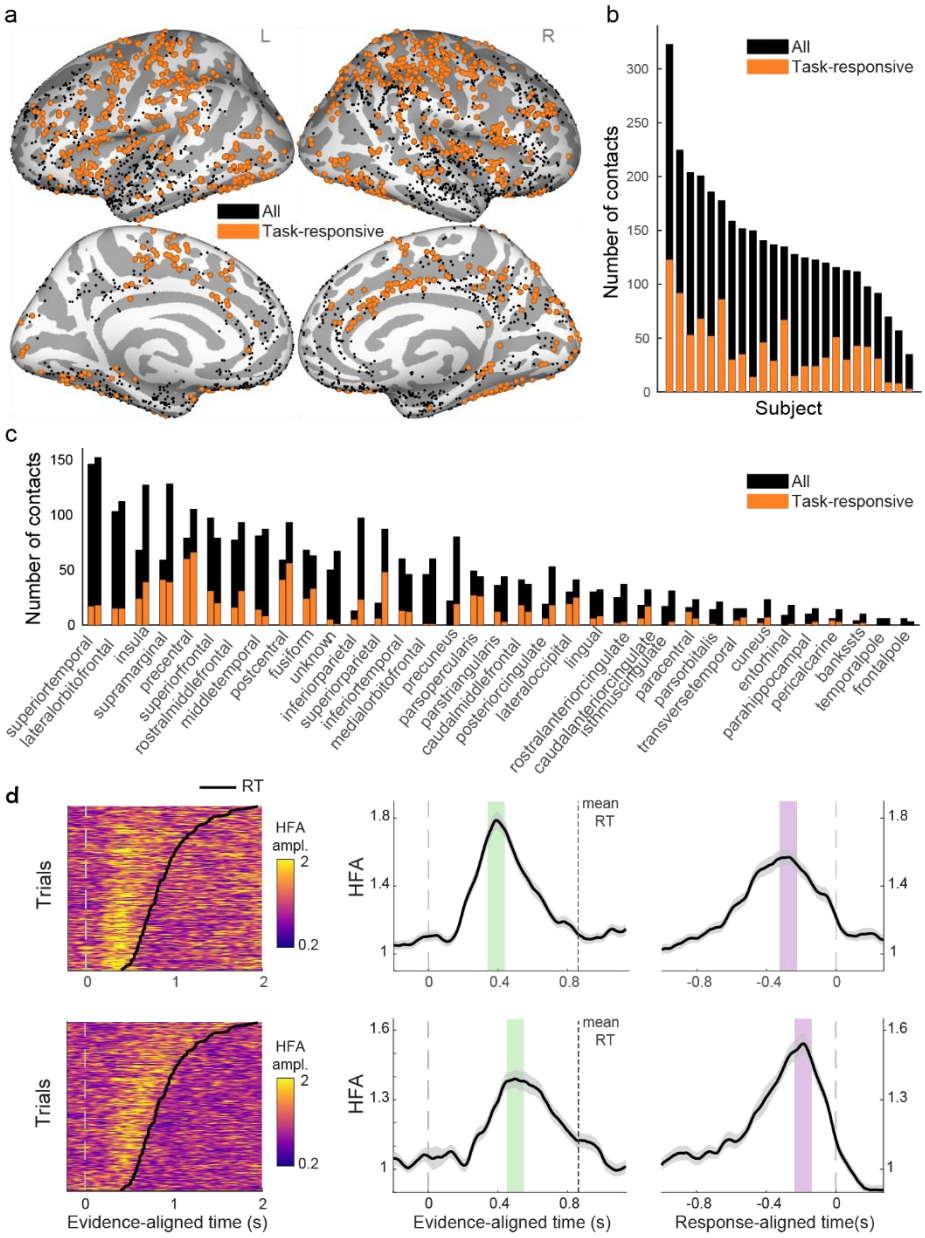

Figure 2. **Overview of coverage and signal profiles for task-responsive contacts.** **a.** Spatial distribution of contacts that exhibited task-responsive activity in the manual response task, defined as a significant increase in HFA following the onset of sensory evidence (i.e., coherent motion). **b**. Number of contacts per subject (black: all contacts included in the analysis, orange: task-responsive sites). **c.** Distribution of contacts across cortical regions. Region labels reflect gyral-based neuroanatomical parcellation[63]. **d.** Activity patterns from two contacts with task-responsive HFA, showing an example of distinct alignment to onset of sensory evidence vs. motor response (top: intraparietal sulcus; bottom: postcentral sulcus; note that these waveforms are included for illustration of temporal alignment as a signal property, and are not meant to be representative of all recording sites in these regions). Color scale represents HFA amplitude. Left: single trial HFA as a function of time. Middle/Right: mean HFA +/- standard error of the mean (SEM) across trials (n=253), as a function of time. Green and violet shaded areas show 100 ms time windows centered on the peak amplitude of the trial-averaged HFA, for evidence- and response-locked data, respectively; HFA amplitudes in the peak-centered intervals was used in subsequent statistical analyses to identify contacts with activity profiles of interest.

We proceeded to categorize task-responsive contacts based on their activity profile, focusing on how HFA at these sites varied with stimulus properties and motor effector. Specifically, for each contact, we assessed whether and how the HFA activity depended on sensory evidence strength, spatial location of the evidence, the side of the motor response, and the alignment to evidence onset (i.e., coherent motion) vs. the time of response, by means of factorial ANOVAs (see Methods).

Our main goal was to localize neural activity consistent with effector-independent evidence accumulation, as distinct from sensorimotor signals and low-level processes related to the detection of sensory changes. To this end, we first looked for activity consistent with the latter two categories.

We reasoned that activity relating to expressing choice (i.e., involving motor planning, selection, and/or execution) would exhibit effector-selectivity at, or near, the time of the motor response. Therefore, we searched for contacts that showed a significant effect of Motor Effector (left vs. right hand) on HFA amplitude, with stronger activity for responses made with the contralateral effector relative to the recording site (thresholded at $p<0.05$, uncorrected). Additionally, we expected that effector-selective activity would be temporally aligned to, and reach peak magnitude at or near the time of motor response, in line with previous reports from monkey electrophysiology and human scalp EEG[5,24] - importantly, this would lead to larger average peak amplitudes in the response-aligned vs. the evidence-aligned trial-averaged data, due to inherent trial-to-trial variability in response times. Thus, we set as an additional criterion a significant effect of Temporal Alignment (i.e., stronger HFA at the time of response-aligned vs. evidence-aligned peak; $p<0.05$, uncorrected). We identified a total of 233 contacts meeting these criteria, which, as expected, were primarily located in sensorimotor regions of the cortex (Fig. 3a, top panel).

We next searched for activity consistent with transient, low-level spatially-selective processes related to the detection of goal-relevant sensory changes (in this case, onset of coherent motion). Such signals have been previously characterized in non-invasive, human EEG[28,32], appearing relatively early after evidence onset and scaling with the strength of sensory evidence. While these early target selection signals share some of the characteristics of evidence accumulation signals, they can be distinguished from them by the fact that they are closely time-locked to evidence onset and lateralized according to the hemifield in which evidence appears. Our behavioral paradigm involving two simultaneous stimuli (one in each hemifield) allowed us to selectively search for activity meeting these characteristics. Thus, we looked for contacts that simultaneously exhibited 1) significant modulation by Evidence Location in the evidence-aligned HFA (with the expectation of stronger activation when the coherent motion was presented on the side contralateral to the contact; $p<0.05$, uncorrected); 2) significant positive modulation by Evidence Strength in the evidence-aligned HFA ($p<0.05$, uncorrected); 3) a significant effect of Temporal Alignment ($p<0.05$, uncorrected), with greater mean amplitude when aligned to the onset of the evidence than to the motor response; and 4) no significant modulation by left/right Motor Effector ($p>.05$, uncorrected). Note that while many of these criteria are also true of sensory evidence-encoding activity such as found in middle-temporal area MT, the temporal-alignment criterion selects against such lower-level encoding because, being sustained for the duration of motion presentation[33], it would not be expected to differ in the stimulus-locked and response-locked timeframes. We found only 2 contacts that met these criteria, located in the inferior temporal gyrus and superior frontal sulcus (Extended Data Fig. 1). As these contacts were so few and situated in more sparsely sampled brain areas, we did not further characterize the activity in this category.

Lastly, we looked for sites that exhibited properties similar to the abstract (motor-independent) accumulation activity observed in scalp EEG. To achieve this, we isolated contacts that simultaneously showed 1) significant modulation by the Evidence Strength in the evidence-aligned HFA ($p<0.05$, uncorrected), whereby stronger motion coherence was associated with higher HFA amplitude at the evidence onset-aligned peak, 2) independence from the limb used to express choice, defined as the absence of a significant main effect of Motor Effector ($p>.05$, uncorrected), and 3) independence from the spatial location of the sensory evidence, defined as the absence of a significant main effect of Evidence Location ($p>.05$, uncorrected). As we do not yet know whether and how the neural representations of the choice alternatives (upward and downward motion directions) are intermingled vs. spatially separated in the cortex, much less whether iEEG could distinguish any such spatial separation, our study was not designed in a way that would allow using direction selectivity as a criterion (i.e., dissociated from effector selectivity). Additionally, while we used temporal alignment to evidence onset and motor response as selection criteria when isolating effector- and target-selective contacts, respectively, we did not do so when localizing candidates for abstract evidence accumulation. Existing literature would suggest that the culmination of the evidence accumulation process tends to be more tightly aligned to the time of motor execution (i.e., with choice commitment being shortly followed by a response), which would

result in the average signal amplitude showing a higher peak in the response-aligned compared to the evidence-aligned data. However, this is not always observed to be the case (e.g., see [34]) and is likely to vary across tasks depending on the proportion of RT variance that is driven by evidence accumulation vs. post-commitment motor execution processes. We therefore did not impose any assumptions regarding the relative degree of alignment to evidence onset vs. response execution when isolating these abstract signals. Under these criteria, we identified 182 contacts, distributed broadly across prefrontal, parietal, ventral temporal, and insular regions (Fig. 3b, top panel). Further inspection of their spatial distribution in relation to intrinsic cortical networks previously estimated based on functional connectivity[35] revealed some overlap with what is commonly referred to as the dorsal attention network (intraparietal sulcus and the junction of the precentral and superior frontal sulcus) and the salience/ventral attention network (dorsal anterior cingulate and orbital fronto-insular cortices)[36,37](Fig. 3c; see anatomical parcellation in Extended Data Fig. 2a). Activity in these sensors grew gradually over time and, on average, peaked at least approximately 200 milliseconds before response execution (Fig. 3b, bottom panel), though this latency varied across subregions (Fig. 3d, Extended Data Fig. 2b), and across individual sites (Fig. 3e, Extended Data Fig. 3a). A larger average amplitude can be observed at the response-aligned peak compared to evidence-aligned peak ($t(181)=2.91$, $p=0.004$, $d=0.11$, 95% CI: [-0.1 0.31] paired-sample t-test, two-tailed), consistent with a representation of decision formation whose peak aligns more with the time of response than the stimulus, as would be predicted when post-commitment motor-related processes are on average less variable across trials than the decision process itself. Having selected these electrodes partly based on the criterion of coherence-dependence in stimulus-locked amplitude, we further verified that the *rate* of build-up in the response-aligned activity increased with coherence across the 182 contacts (Fig. 3f). We compared build-up rates associated with the two motion coherence conditions by performing one-tailed paired t-tests across contacts, under the prediction of steeper build-up rates for the High coherence condition. Indeed, we found that across contacts in this category, activity buildup was reliably modulated by evidence strength ($t(181)=-6.31$, $p<0.001$, $d=0.48$, 95% CI: [0.28 0.69]; only correct choices included in this analysis; Fig. 3f, top panel). Meanwhile, in the effector-selective category of electrodes, this effect was not significant across contacts ($t(232)=-1.18$, $p=0.24$, $d=0.02$, 95% CI: [-0.16 0.2]; only correct choices were included in this analysis, Fig. 3f, bottom panel) (though further analysis of single-trial activity at individual contacts did reveal a small number of sites with significant buildup modulation; n=39/233, thresholded at $\alpha=.05$, one-tailed test).

Note that using a more similar set of criteria for effector-selective vs. abstract accumulator profile categories (i.e., by including requirements for Evidence Strength modulation and absence of Evidence Location selectivity in the selection of effector-selective contacts) resulted in a reduction of the number of qualifying contacts (N=92) but did not change the outcome of follow-up analyses (Extended Data Fig. 4).

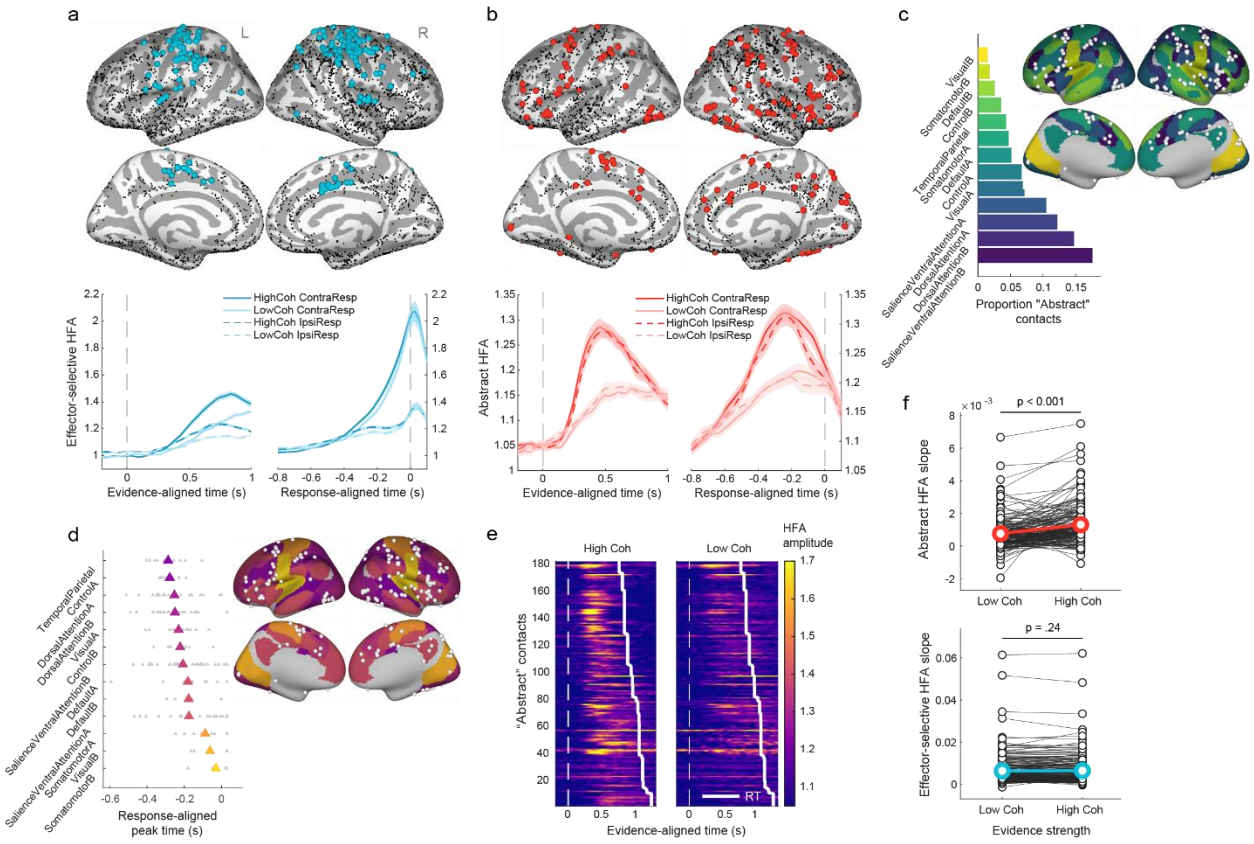

Figure 3. **Mapping signal profiles of interest.** Spatiotemporal profile of HFA consistent with: **a.** effector-selective, mainly response-aligned activity and **b.** abstract (effector-independent) activity. *Top:* Spatial distribution (colored dots: sites meeting criteria for activity profile of interest; black dots: all sites included in the analysis). Electrodes have been projected onto the Freesurfer[59] average inflated brain (light gray: gyri; dark gray: sulci). *Bottom:* Temporal profile of mean HFA across contacts, separated by strength of sensory evidence (High vs. Low motion coherence) and effector laterality (contralateral vs. ipsilateral hand response). Shaded areas in **a** and **b** represent +/- SEM across contacts. Note that some basic features of these waveforms were guaranteed by the electrode selection criteria, most notably the dominance of contralateral- over ipsilateral-hand activity for the effector-selective electrodes (**a**) and the stronger stimulus-locked amplitude for high- vs. low-coherence trials in the abstract category (**b**). These plots lay out the average temporal dynamics in these electrodes in full. **c.** Proportion of sites categorized as "abstract" across intrinsic cortical networks (calculated relative to the total number of recorded sites in a given network). **d.** Average time of peak HFA amplitude relative to motor response, across intrinsic cortical networks. Gray symbols reflect values at individual contacts. Parcellations in **c** and **d** represent networks estimated on the basis of resting-state functional connectivity[37]. Only parcels with coverage of at least 5 contacts are displayed. **e.** Temporal profile of HFA at individual sites categorized as abstract accumulator candidates, separated by strength of sensory evidence. **f.** Modulation of response-aligned buildup rate by motion coherence for abstract accumulator candidate sites (top) and effector-selective sites (bottom). Each pair of data points represents an individual contact. The slopes of the HFA buildup were computed by fitting a straight line to the trial-averaged trace, separately for each motion coherence level, in a 300 ms time window ending at the response-aligned peak HFA amplitude (with peak amplitude identified within the -600 to 30 ms time interval relative to motor response). For electrodes categorized as effector-selective, the buildup rate comparison was performed using only trials associated with the contralateral motor response. P-values were derived from two-tailed, paired-samples t-tests.

Relationship between decision-related HFA and behavior. Having located candidate abstract evidence accumulation signals on the basis of sensitivity to key task components, we sought to further investigate their relationship with choice performance, employing criteria that did not inform their initial identification. Non-invasive EEG recording studies have highlighted a dissociation in the way that effector-selective and abstract evidence accumulation signals relate to choice behavior. Whereas effector-selective signals reach a fixed amplitude at response irrespective of accuracy or RT, the amplitude of abstract cumulative evidence signals prior to the behavioral response is reduced in the same trials where accuracy is reduced: in the very fastest RT trials (potentially due to starting point variability including that caused by any premature accumulation of sensory noise[38]), and beyond these fastest trials, reducing again with increasing RT [27,30]. This latter feature has been shown to accord with the operation

of evidence-independent 'urgency' signals at the motor level that progressively reduce the cumulative evidence required to trigger action[27,30,36,37], observed especially when response deadlines are imposed. To establish whether a similar dissociation was evident in the present data, we first calculated conditional accuracy functions (CAF) by dividing trials into six RT bins for each subject and computing the proportion of correct responses in each bin. With the exception of the fastest RT bin, accuracy tended to decrease monotonically with increasing RT (5x2 repeated-measures ANOVA on the proportion of correct responses across the five fastest RT bins within each motion coherence condition, $F_{RT}(4,80)=15.49$, $p<0.001$, partial $\eta^2 = 0.43$, 95% CI: [0.25 0.54], Fig. 4a, top panel).

As predicted, for abstract accumulator candidates, the pattern with which peak HFA amplitude in the response-aligned signal varied with RT (Fig. 4b, top panel) mimicked the pattern observed in the conditional accuracy function, with a reduction for the fastest RT bin, and beyond the middle bins, decreasing as a function of RT (5x2 repeated measures ANOVA on HFA amplitude: $F_{RT}(4,628) = 25.98$, $p < 0.001$, partial $\eta^2 = 0.14$, 95% CI: [0.09 0.19]). We verified this similarity by computing Pearson's correlations between the RT-binned pre-response HFA and corresponding choice accuracy, separately for each channel. To assess whether the average correlation across channels in this category was significantly higher than chance, we generated a null distribution by computing the average correlation coefficient after shuffling the order of HFA bins, and repeating this procedure 5000 times. Indeed, we found that RT-binned HFA correlated significantly with accuracy across contacts (mean r = .32, $p<0.001$, from permutation test). This pattern is in line with an abstract decision-related evidence accumulation signal where slower, less accurate decisions are made based on smaller amounts of cumulative evidence. In contrast, in sites characterized by effector-selective activity (Fig. 4, bottom panels), correlation with the CAF was not significant (mean r = .09, p=0.19, from permutation test; Fig. 4b, bottom panel) and was lower than that observed for HFA from abstract accumulator candidates ($t(343)=6.32$, $p<.001$, $d=0.68$, 95% CI: [0.46 0.9], two-tailed t-test on Fisher's z transformed correlation coefficients). Similarly, the decrease in HFA amplitude with slower RTs was significantly weaker at these sites (2x2 mixed ANOVA with factors Contact Category and Motion Coherence on the rate of HFA decrease with RT, i.e., slopes obtained from fitting a straight line to the average HFA associated with the five slowest RT bins; $F_{CATEGORY}(1, 312)=19.52$, $p<0.001$, partial $\eta^2 = 0.06$, 95% CI: [0.02 0.12]).

We also observed higher amplitudes for correct responses than for errors in the HFA from abstract accumulator candidates, in line with errors being based on less cumulative evidence (2x2 repeated-measures ANOVA across contacts, with factors Motion Coherence and Accuracy; $F_{ACC}(1, 139)=55.32$, $p<0.001$, partial $\eta^2 = 0.28$, 95% CI: [0.17 0.39] ; Fig. 4c, top panel). Interestingly, this effect was also present in the effector-selective HFA ($F_{ACC}(1,130)=73.32$, $p<0.001$, partial $\eta^2 = 0.36$, 95% CI: [0.23 0.47]), although given that activity at these locations tended to peak at or even after motor response, it is possible that the higher amplitudes observed here for correct choices might be related to fluctuations in motor execution (e.g., vigor of response).

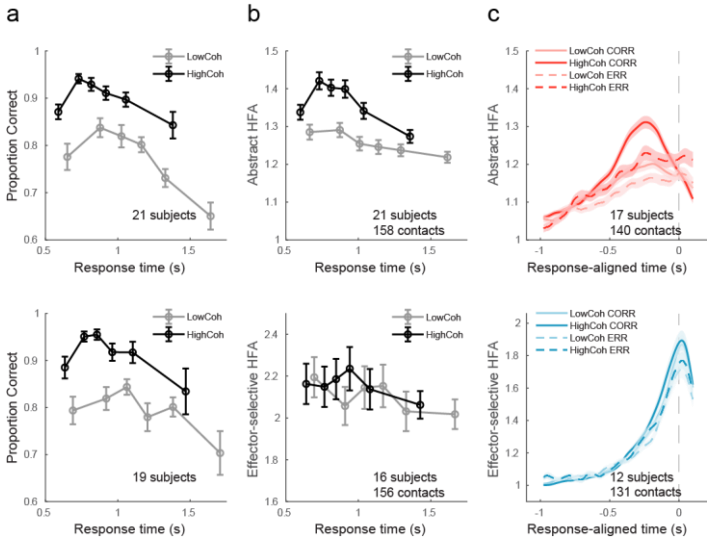

Figure 4. Relationship of HFA with decision-related behavior. Top and bottom panels represent data corresponding to the effector-independent (abstract) and effector-selective electrodes, respectively. **a.** Conditional accuracy function:

choice accuracy as a function of response time bins, separated by the strength of sensory evidence (i.e., motion coherence). The y axis shows the mean accuracy across subjects, weighted by the number of contacts that contributed to each subject's data +/- weighted SEM across subjects. **b.** HFA at the response-aligned peak, as a function of response time bins. The y axis shows the average HFA across all contacts in a given electrode category. Only trials associated with correct choices were used for this analysis. Data points are presented as mean values +/- SEM across contacts. **c.** Response-aligned average HFA traces, separated by choice accuracy and evidence strength. Shaded areas represent +/- SEM across contacts. Note that panels **b** and **c** reflect data only from subjects with a minimum of 5 trials available per bin. For electrodes categorized as effector-selective, only trials associated with the contralateral motor response were included in these analyses.

Vocal response task. Although we made efforts to isolate potential generators of abstract evidence accumulation from effector-selective activity by excluding sites that exhibited limb selectivity, it is nevertheless conceivable that activity at some of these locations could be movement-dependent in a way that is not selective to the limb used to respond. Thus, to provide additional support for motor independence in our candidate sites, we examined recordings from a subset of participants who performed an alternative version of the task (Fig. 1a), where requirements for modality and timing of response were modified (Methods). Specifically, subjects were asked to report their choice vocally, and to do so only after a forced random delay (1000-2000 ms) marked by a visual cue.

Behavior. Subjects (N=12) responded correctly on 88.28% of the trials (SD=8.05%). Choice accuracy was not significantly different from the manual response task (t(11)=1.11, p=0.291, *d*=0.46, 95% CI: [-0.33 1.24], paired-sample test, two-tailed). Similarly to the manual response task, behavioral performance was modulated by the strength of sensory evidence, with subjects responding correctly more frequently on trials with strong sensory evidence (Low coherence: M=81.53% correct, SD=11.84%; High coherence: M=94.87%, SD=4.89%; t(11)=4.82, p<.001, *d*=1.42 , 95% CI: [0.53 2.29], paired-sample test, one-tailed) (Fig. 1c).

iEEG. We inspected data from the 12 subjects who took part in both the motor and vocal response tasks. Of the 182 sites identified as candidates for effector-independent evidence accumulation in the manual response task, 111 were also recorded from during the vocal response task (Fig. 5a, Extended Data Fig. 5). We sought to investigate whether activity at these locations continued to display signature characteristics of evidence accumulation despite the change in motor requirements. Indeed, we continued to see an increase in HFA after the onset of sensory evidence, as well as modulation of amplitude by the strength of sensory evidence in 54 (i.e., 48.6%) out of 111 contacts (evaluated within a 100ms time window centered on the evidence-aligned peak; thresholded at p<0.05, uncorrected; see Methods). This pattern was observed irrespective of the order in which subjects completed the two tasks (Extended Data Fig. 6). Additionally, the magnitude of evidence strength modulation at these sites tended to be consistent across the two tasks, as revealed by a correlation on the evidence strength effect sizes (r(109)=.46, p<0.001, 95% CI: [.3 .6], Extended Data Fig. 7). For completion, the extent of overlap in evidence strength modulation between the two tasks is shown across the common electrodes in Extended Data Fig. 7.

We performed the same comparison for sites we previously identified as showing effector-selective activity (Fig. 5b). Neural recordings during the vocal task were available for 84 of the 233 of these contacts. As expected of effector-selective signals, these regions no longer exhibited a neural response to the onset of the sensory evidence or amplitude modulated by the strength of the evidence. Activity at only 9 (i.e., 10.7%) out of the 84 sites continued to show modulation by evidence strength in the vocal task (thresholded at p<0.05, uncorrected). Although absence of evidence cannot be interpreted as evidence of absence, the scarcity of contacts with task responsive and/or evidence dependent signals in this category (compared to the Abstract category) suggests that if these sites support the decision process, the majority do so in a manner that is closely tied to the motor action associated with the choice.

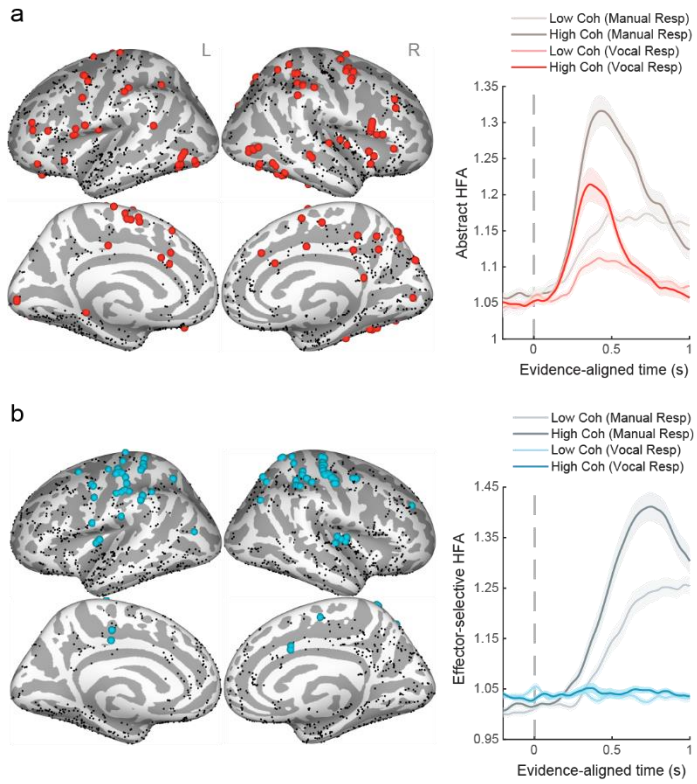

Figure 5. Validating effector independence at "abstract" candidate sites. Top and bottom panels show HFA during the delayed vocal response task in sites previously categorized as **a.** Abstract (i.e., independent of hand response laterality) and **b.** Selective for effector laterality, respectively. *Left panels*: Black dots show contact coverage during the vocal response task. Colored dots mark contacts where neural recordings were made during both the manual and vocal response tasks, and which met categorization criteria in the analysis of the manual response task data. *Right panels:* Temporal profile of average HFA, shown separately for data recorded during the speeded manual response (gray) vs. vocal response task (color), and separated by strength of sensory evidence (High vs. Low motion coherence). Shaded areas represent standard error of the mean across contacts.

Discussion

Localizing the brain regions involved in the formation of movement-independent perceptual decisions is a long-standing challenge in decision research. By exploiting the spatiotemporal precision of intracranial EEG, our study sought to provide a more extensive spatial mapping of abstract decision-related signals in the human brain than was previously available. We identified a broadly distributed network where activity exhibited characteristics consistent with abstract representations of evolving perceptual decisions. Specifically, we observed a gradual build-up following the onset of sensory evidence, at a rate that scaled with the quality of the evidence and reflected both subjects' choice accuracy and response times. Crucially, these signals were insensitive to the evidence location and laterality of the motor effector. Key to our approach was the ability to further validate the independence of these decision-related signals from movement requirements using an independent data set, showing that activity continued to trace cumulative evidence irrespective of whether participants responded via a speeded manual button push or delayed vocalization.

Our results highlight abstract, evidence-dependent decision dynamics in the human brain which have previously only been observed using non-invasive methods characterized by high temporal but relatively poor spatial precision[41,23,24]. Our approach allowed us to not only capture the focal activity that might have been missed with scalp EEG, but to sample from multiple regions across the brain from our large sample of participants. The spatial distribution of the abstract accumulation dynamics observed in our data included prefrontal, parietal, inferior temporal, and anterior insular regions. Not surprisingly, several of these regions have been previously implicated in effector-independent decision processes, by work involving human neuroimaging (prefrontal cortex, PFC[16], anterior insula[13,14], inferior temporal[42]), and single unit recordings in humans (parietal[43]) and non-human primates (PFC[10], parietal[9]), though none of these studies identified all of these activations at once.

The profile of activity at the abstract accumulator candidate sites identified here was consistent with human scalp EEG signals previously shown to exhibit evidence accumulation dynamics in an effector-independent manner[25,29,30,34,44]. A question arising from this observation is whether our data highlight potential neural generators of such CPP-like signals. It should first be noted

that the local dynamics responsible for voltage fluctuations measured with scalp EEG are likely distinct from those underlying the HFA measurements obtained from intracranial recordings. Specifically, while event-related potentials reflect relatively slow fluctuations in the broadband signal arising primarily from dendritic postsynaptic potentials[45], intracranially recorded HFA has been shown to correlate, at least in part, with neuronal spiking activity[46,47]. Thus, to the extent that activation in any given area would tend to give rise to both spiking and postsynaptic activity, it is plausible that one or more of the areas identified here contribute to the scalp-measured CPP, though the degree of the overlap remains speculative for now. Future work employing simultaneous recordings of scalp and intracranial EEG and/or source modeling may provide further insight into this question.

The relationship of the neural signal with stimulus properties and behavior in the period just before overt choice commitment has important implications for interpreting the quantity represented at these locations. Specifically, we showed that, in keeping with observations of the scalp-recorded CPP, the peak amplitude of the neural response scaled with the strength of the sensory evidence, as well as with response speed and decision accuracy. This pattern differs from what is typically observed in movement-selective regions, where activity reaches a fixed threshold prior to choice irrespective of stimulus properties or behavior[3,48]. Insight into the origin of this difference comes from work investigating decision dynamics under varying speed pressure conditions. Specifically, it has been proposed that in the context of speeded perceptual decisions (i.e., where a choice deadline is imposed), an additional time-dependent "urgency" signal may contribute to elevating the decision variable to an action-triggering boundary in areas of the brain responsible for planning and preparing the appropriate movement[39,40,49,27], such that smaller amounts of cumulative evidence are necessary for committing to a choice as time elapses. According to this view then, abstract evidence accumulation signals like the CPP and the iEEG signals isolated in the present study reflect the cumulative evidence informing the choice at the time of commitment which varies as a function of urgency. In contrast to the abstract accumulator candidates, activity at the effector-selective sites was more in line with a boundary-crossing process, with activity reaching similar amplitudes regardless of the amount of sensory evidence. However, unlike movement-selective evidence accumulators in the non-human primate brain, where response-aligned activity also reflects the steeper buildup rate for easier choices, we did not, on average, see such an effect in this group of contacts. This could be because our effector-selective criteria would identify not only signals related to motor preparation, to which there is a continuous flow from evidence accumulation, but also signals related to motor execution and/or somatosensory feedback, which would be more tightly response-aligned, stereotyped, and possibly dominant over motor preparation signals. Indeed, non-invasive neurophysiology work has shown that motor preparation signals tend to be reflected more reliably in lower frequency bands whereas higher frequency responses tend to be more response-aligned and stereotyped, similar to what we found using intracranially recorded HFA[50]. Thus, the type of effector-selective activity identified here cannot be directly compared to the movement-selective evidence accumulation identified with monkey electrophysiology in areas such as the LIP, where any single-unit activity purely related to motor execution or somatosensory feedback would typically be excluded from the analysis.

Interestingly, the activity at our abstract accumulator candidates differed from that of CPP-like EEG signals in terms of its timing relative to choice commitment. Average HFA in our study peaked considerably earlier (i.e., 200-300 ms prior to motor response) than the CPP which is typically observed to peak at, or just prior to the response. One possible explanation is that the scalp-recorded CPP may contain a mixture of both abstract evidence accumulation and motor-related signals (planning/execution). As we excluded sources of effector-selective activity in our analysis, our data may reflect a more precise temporal profile of abstract decision formation, whereby the culmination of abstract evidence accumulation precedes that of motor-related processes. Simultaneous intracranial and scalp recordings could allow future work to directly compare the peak latency in signals identified here vs. the CPP, and to use scalp-recorded motor potentials to index post-decisional delays (see Kelly et al 2021), thus further examining this possibility. Alternatively, the time between choice commitment and motor execution might have been longer for our patient sample due to limited training and time on the task compared to the typical experiments performed in healthy volunteers.

It remains to be determined whether the regions identified here form a homogenous network serving a common, causal role in the decision process or whether they have unique contributions. For instance, several of the regions where we identified abstract evidence-dependent activity have been previously implicated in salience and attention related processes (Fig. 3d). This is perhaps not surprising in that manipulations commonly applied to identify such attention networks would also differentially activate decision processes (e.g., a decision is required to interpret an attentional cue, but not for passive viewing of the same cue). However, while the aggregate dynamics of the abstract sites adhere much more obviously to the well-defined properties of

evidence accumulation (e.g. it is not clear why attention would be reduced in both the fastest and slowest RT trials), it cannot be entirely ruled out that some portion of these electrodes or the activity measured at them reflect an attention-related function. It will therefore be important for future studies to examine which of these regions play causal roles in the evidence accumulation process, as opposed to merely tracking the cumulative evidence. Relatedly, while the representations uncovered here are independent of the specific motor effectors required by our experimental paradigm, our study cannot fully rule out that activity at some of the identified locations may still reflect non-abstract accumulation, for instance if subjects used alternative strategies for representing and/or storing choices that involve (real or imagined) motor activity unrelated to task requirements. We took measures to minimize this possibility, such as counterbalancing the order of response types and choosing up/down motion rather than left/right, the latter of which would more naturally map to lateralized movements. The data can at least rule out that evidence in the vocal task is being accumulated in the same effector-selective neurons as the button-press movements, based on the lack of HFA buildup in the effector-selective electrodes during the vocal task. Furthermore, if a latent movement plan is being recruited specifically to perform the vocal task, this motor-related activity might be expected to show a similar evidence-locked temporal profile to the known effector-selective sites identified in the manual task, whereas our abstract accumulator candidates appear to peak earlier, on average. Finally, it should be kept in mind that applying statistical criteria for categorizing signal profiles as we have done here always comes with a certain risk for mis-categorization, and type-II error risk in particular would be reduced with increased statistical power. Thus the abstract, effector-independent nature of the accumulation activity (detected initially here by non-significance of effector) cannot be definitively concluded for each and every contact identified. Rather the analyses provide strong candidate sites for future investigations with other techniques. Studies able to perturb neural activity during evidence accumulation (e.g., intracranial electrical stimulation[51]) will be better suited to address these questions.

Also worth considering is that, although we recorded from a large participant sample with substantial bilateral coverage of all cortical lobes, our study is subject to a limitation inherent to all intracranial studies, namely heterogeneous electrode coverage across patients due to electrode locations being determined solely based on clinical purposes. It is therefore possible that our study could have missed decision-related signals originating in regions not sampled from, for instance subcortical structures such as the basal ganglia[52,53], which have previously been implicated in evidence accumulation.

Methods

Participants. We recorded data from neurosurgical patients suffering from drug-resistant epilepsy and undergoing intracranial EEG (iEEG) monitoring at the North Shore University Hospital (Manhasset, NY 11030, USA), aimed at locating seizure foci and informing treatment. The study was approved by the institutional review board of the Feinstein Institutes for Medical Research (protocol number 07-125). All participants provided written informed consent in accordance with the Declaration of Helsinki. No compensation was provided for taking part in the study.

24 participants (12 female, age range 18-57, M=35.8 years) took part in the speeded manual response version of the random dot task. Of these, 12 (5 female, age range 18-57, M=38.25 years) additionally performed a delayed vocal response version of the task. To control for learning effects across the two tasks, we alternated the order of the two tasks, such that 5 out of 12 subjects performed the vocal version first, while the remaining 7 subjects performed the manual version first.

Stimuli and tasks. Stimuli were presented at bedside using the Psychophysics Toolbox version 3 for MATLAB (Mathworks, Natick, MA). Stimuli consisted of two simultaneous random dot kinematograms (white dots on black background) presented within circular apertures that were placed symmetrically on the left and right of a central fixation dot (Fig. 1a). At the onset of the dot stimuli, motion on both sides was incoherent. After a random delay (1.4-1.8 s, uniformly distributed), motion on one unpredictable side of the fixation became coherent towards one of two possible directions (up or down). Coherent motion lasted for 2 s. The transition from incoherent to coherent motion served to minimize the extent to which sensory evoked potentials to visual changes might obscure decision-related activity. Subjects were asked to determine the direction of the coherent motion, irrespective of the side it was presented on. Performance feedback was provided at the end of each trial: “Correct”/“Wrong” if a response was made during the allocated time window, “Too early” if a response was made before dot motion became coherent

(i.e., before the onset of sensory evidence), or "No response?" if a response was not made or missed the deadline. Feedback was displayed for .4 s and was followed by an inter-trial interval of 1 s (blank screen).

Difficulty of the random dot stimuli was determined by the proportion of dots moving coherently in one direction (i.e., motion coherence) and was calibrated separately for each subject during a practice session prior to the main experiment. We used two motion coherence levels, adjusted to span perceptual peri-threshold. Specifically, subjects performed short trial blocks and difficulty was gradually adjusted after each session until performance, when averaged across the two difficulty levels, remained consistent at around 75-80% correct. Motion coherence for the difficult condition was adjusted to half of the value of the easy condition. The average proportions of coherently moving dots for the Low and High coherence conditions across the 24 subjects were .28 and .56, respectively. All stimulus conditions (evidence presentation side, motion coherence, and motion direction) were equally and randomly distributed across trials. For subjects who took part in both versions of the task, training was done on the task type that the subject performed first (i.e., Vocal responses for the Vocal task, manual responses for the Manual task). This served to avoid any potential associations between perceptual choice and the alternative response modality in the task performed first.

Speeded manual response task. On each trial, participants reported their choice by making a button press with their left or right hand using a mouse. The two possible motion direction choices were each assigned to one motor effector (left or right limb), and this mapping was maintained throughout the entire experiment. Choice-effector mapping was counterbalanced across subjects (11/24 subjects responded with right hand to report upward motion). Subjects performed between 3-6 blocks of 64 trials each (average number of trials per subject: 256). Motor responses were allowed only during the time window where coherent motion was present. Trials where responses were given outside of this time range were excluded from further analysis (mean proportion of missed trials across subjects = 9.17%; SD=7.88%, where 0.9% were due to premature responses made before motion became coherent).

Delayed vocal response task. The vocal version of the task was identical to the motor version, with two exceptions: 1) subjects were instructed to wait through a random delay (1-2 s, uniformly distributed) for a visual "go" cue before reporting their choice, which was marked by a change in the fixation color from white to green; 2) choices were reported vocally by naming the direction of the dots out loud (e.g., "Up" or "Down"). The experimenter pressed the appropriate mouse button according to the subject's vocal response, and this was immediately followed by visual feedback ("Correct"/"Incorrect"). Vocal answers were also recorded for all subjects. Subjects performed between 3-4 blocks of 64 trials each (average number of trials per subject: 245).

iEEG data acquisition. Patients were implanted with either depth (2- or 1.3-mm platinum cylinders with 4.4- or 2.2-mm center to center distance and a diameter of 0.8 mm; PMT corporation, Chanassen, MN) and/or subdural strip/grid electrodes (2- or 3-mm platinum disks with 4- or 10-mm center to center distance; PMT corporation, Chanassen, MN). The placement of the electrodes was determined exclusively based on clinical considerations. Intracranial data were recorded using either an XLTEK Quantum Amplifier (Natus Medical Inc., San Carlos, CA) at 1 kHz (i.e., in 12/24 subjects for the Manual task and 6/12 subjects for the Vocal task), or a Tucker-Davis Technologies acquisition module controlled by software package Synapse (Tucker-Davis Technologies, Alachua, FL), at 3 kHz. The iEEG signal was referenced online to a reference electrode located either subdurally, subdermally, or in the white matter, which was determined upon visual inspection of the signal quality, at the bedside. Transistor–transistor logic (TTL) pulses triggered by the stimulus presentation software at events of interest were recorded simultaneously with the iEEG data, which subsequently served to align intracranial recordings to task-related events of interest.

Electrode localization. Electrode localization and visualization was performed using the iELVis toolbox[54] for MATLAB. Prior to electrode implantation, a T1-weighted 1-mm isometric structural magnetic resonance imaging (MRI) scan was acquired for each subject, on a Siemens 3T MRI scanner. After electrode implantation, a computerized tomography (CT) scan and a T1-weighted MRI scan were acquired. The post-implantation CT and MRI scans were co-registered to the preoperative MRI scan using FSL's BET[55] and FLIRT[56,57] algorithms. Co-registration of these two scans allowed us to minimize localization error caused by potential brain shift and to visualize the CT scan on top of the preoperative MRI. Semi-manual identification of contact artifacts on the co-registered CT was done in BioImageSuite[58]. Volumetric information from the preoperative T1 scan was obtained using the "recon-all" command in Freesurfer[59] v6.0.0. For visualization on the inflated brain surface, depth electrodes were snapped to the nearest point on the Freesurfer pial surface.

Data preprocessing. We recorded data from a total of 5636 intracranial sites across all participants. Contacts that displayed abnormal epileptiform activity or were located within seizure onset zones (as assessed by the clinical epileptology team), as well those found outside of the brain tissue, were excluded from further analysis. iEEG time series were then visually inspected for signal quality, and any electrodes containing systematic artifacts or interictal spikes were also discarded. This led to the exclusion of 1572 contacts. Finally, we excluded contacts located fully in white matter tissue, using the proximal tissue density (PTD) measurement[60] as a criterion. The PTD represents the normalized difference between gray and white matter voxels surrounding the contact centroid (where min/max values of -1/1 reflect tissue composition of only white and only gray matter, respectively). To maintain a conservative approach to electrode exclusion, we removed only those for which PTD<-0.9 (N=684 contacts). Overall, a total of 3380 contacts across all subjects were considered for further analysis (Fig. 1a). These consisted of 2946 depth, 273 grid, and 161 strip contacts. Data were resampled to 512 Hz. Additionally we applied notch-filters at 60 Hz, 120 Hz, and 180 Hz. Lastly, data were re-referenced to the average of all electrodes that passed the quality check. We epoched the data from -3 to 3s relative to the onset of the sensory evidence (i.e., coherent motion). Trials containing strong transient artifacts were manually removed based on visual inspection. Additionally, we removed trials where response times were shorter than 250ms (on average 0.9% of trials).

HFA analysis. To extract high frequency activity (HFA), we bandpass filtered the preprocessed signal in non-overlapping 10Hz bands from 70 to 170 Hz (using Matlab "filtfilt"; 4th order butterworth). We then applied the Hilbert transform to the filtered signal and extracted the instantaneous amplitude from the resulting analytic signal. The instantaneous amplitude for each frequency band was normalized by division to the average of the time series, then averaged across the ten frequency bands to obtain a single time series, and finally squared to extract power.

Selection of task-responsive contacts. Task-responsive sites were defined as those that exhibited an overall increase in HFA during the "decision period" (i.e., the time interval starting 200 ms after evidence onset and ending at the subject-specific median response time), relative to a pre-evidence baseline period (-450 ms to -50 ms prior to onset of the coherent motion), as assessed with a one-tailed t-test on time-averaged HFA (α=.01, one-tailed t-test). The decision to look for HFA responses after 200 ms was informed by previous work showing that changes to the physical evidence (e.g., onset of coherent motion) begin to impact on the build-up of decision signals around this time point[24,30,61].

Identification of contacts with activity profiles of interest. For data acquired during performance of the manual response task, we examined the relationship between HFA and three task-related variables of interest: 1) the strength of sensory evidence of the random dot stimulus (i.e., High vs. Low motion coherence), 2) the motor effector used to report choice (i.e., Ipsilateral vs. Contralateral limb, relative to the recording site), and 3) the spatial location of the sensory evidence (Ipsilateral vs. Contralateral side of the visual fixation). We simultaneously assessed these effects in the evidence-aligned and response-aligned data. Specifically, for each contact, we extracted the mean HFA within a 100ms window centered on the peak of trial-averaged activity, separately for evidence- and response-aligned data. For evidence-aligned data, selection of the average peak was made from the interval starting 200ms after evidence onset and up to 100 ms after the subject's median RT. For response-aligned data, the peak search interval started 600ms before, and ended 30 ms after motor response. We conducted a 2x2x2x2 mixed model ANOVA on these measurements, with between-unit factors: Evidence Strength (High/Low), Motor Effector (Ipsilateral/Contralateral Limb), Evidence Location (Ipsilateral/Contralateral Side), and within-unit factor Temporal Alignment (Evidence-/Response-aligned). For effects that were predicted to be specific to waveforms aligned to one of the two task events (e.g., evidence onset), significance thresholds were based on a separate 2x2x2 ANOVA conducted on that subset of data (see Results).

Follow up statistical analyses on Abstract and Effector selective sites. Further validation of the signal characteristics for these two contact categories was done using conventional ANOVA/t-test approaches. Note that these additional analyses were done across contacts from all participants, i.e., without accounting for potential variability between subjects or between different brain regions. While multilevel statistics can be more robust by accounting for dependency across samples (in this case, HFA from individual contacts)[62], such an approach was also not ideal for the current dataset due to the very low number of contact contributions from some subjects/regions (as little as one) making it difficult or impossible to tease apart variance associated with the experimental condition vs. the subject/region itself in those cases.

For data acquired during the vocal response task, we assessed modulation by evidence strength with a 2x2 ANOVA on evidence-aligned HFA, with factors Evidence Strength and Evidence Location. The 100ms time window of analysis for each electrode was selected under the same parameters as above, using subject-specific median RTs from the manual response task as estimates for the end of the decision period.

Statistics & Reproducibility. No statistical methods were used to pre-determine the sample sizes, however the our sample sizes are similar or larger compared to previous publications where intracranial EEG was used to study cognitive processes, and are comparable to sample sizes used to investigate neural signatures of movement-independent decision formation using non-invasive methods (see literature cited in the Introduction section). Data collection and analysis were not performed blind to the conditions of the experiments.

Extended data

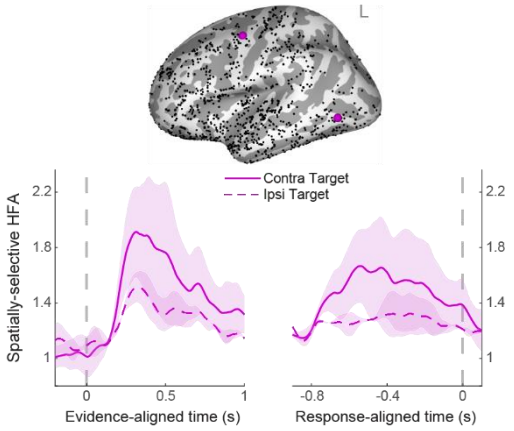

Extended Data Fig. 1. Spatiotemporal profile of HFA consistent with transient low-level spatially-selective processes. *Top:* Spatial distribution of electrodes in this category (black dots: all sites included in the analysis). *Bottom:* Temporal profile of activity, separated by strength of sensory evidence (High vs. Low motion coherence) and spatial location of the evidence (Contralateral vs. Ipsilateral side), averaged across contacts. Shaded areas represent standard error of the mean across contacts.

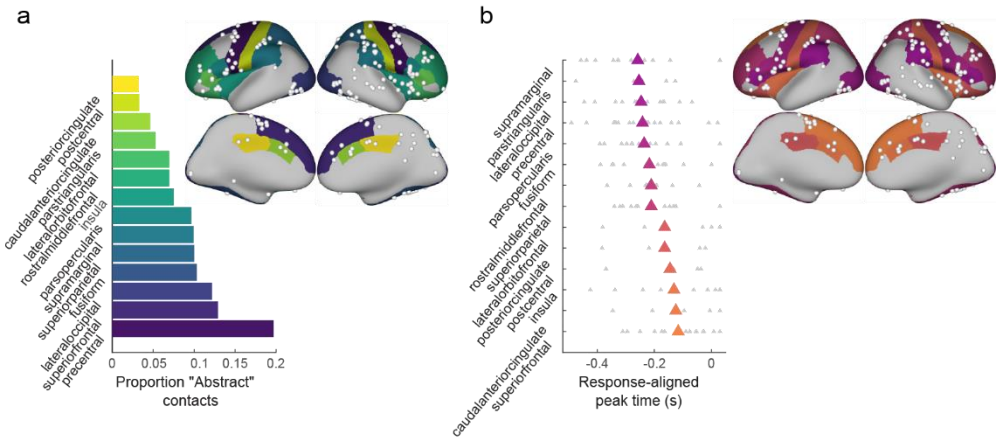

Extended Data Fig. 2. Spatial distribution and temporal variability of sites categorized as abstract accumulator candidates. a. Proportion of sites categorized as "abstract" across anatomical regions (calculated relative to the total number of recorded sites in a given region). **b.** Average time of peak HFA amplitude relative to motor response, by anatomical region. Gray symbols reflect values at individual contacts. Colored brain areas in **a** and **b** represent gyral based parcellations[63]. Only parcels with coverage of at least 5 contacts are displayed.

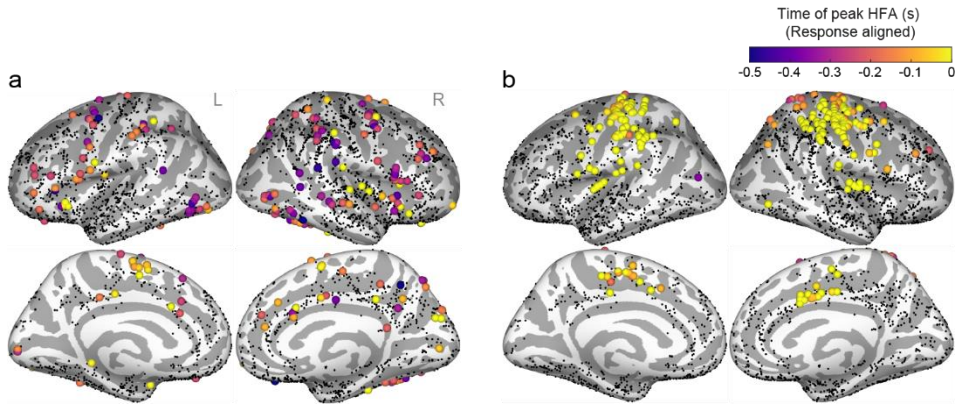

Extended Data Fig. 3. Time of peak amplitude in response-aligned HFA at individual electrodes. a. Abstract (i.e., effector-independent) accumulator candidate sites **b.** Effector-selective sites.

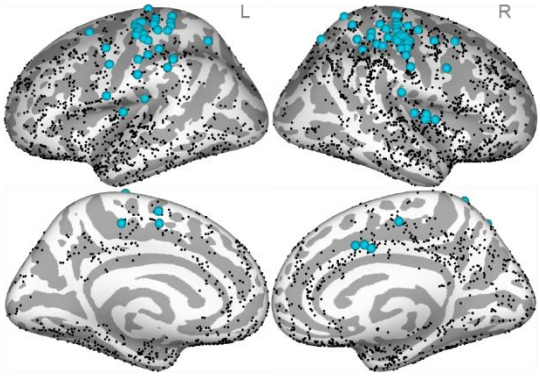

Extended Data Fig 4. Spatial distribution of electrodes categorized as effector-selective under an alternative set of criteria. To isolate this category of contacts (blue dots), we included two additional requirements in the selection criteria which were used for the selection of Abstract accumulator candidates, namely modulation of HFA by Evidence Strength, and the absence of Evidence Location effect. Black dots mark all sites considered for this analysis.

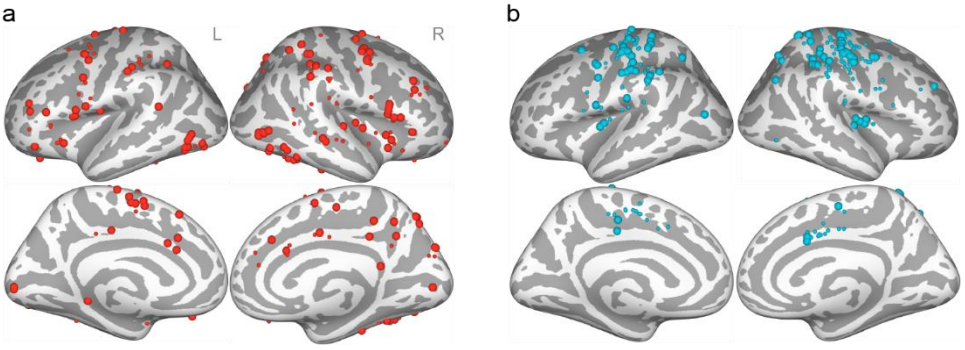

Extended Data Fig. 5. Coverage of sites of interest during the vocal response task. a. Electrodes categorized as potential abstract (i.e., effector-independent) accumulators based on analysis of signals recorded during the manual response task. Small dots mark sites that were recorded from only during the Manual task. Large dots mark the subset of these electrodes which were also recorded from during the vocal response task. **b.** Electrodes categorized as effector-selective. Conventions are the same as in (**a**).

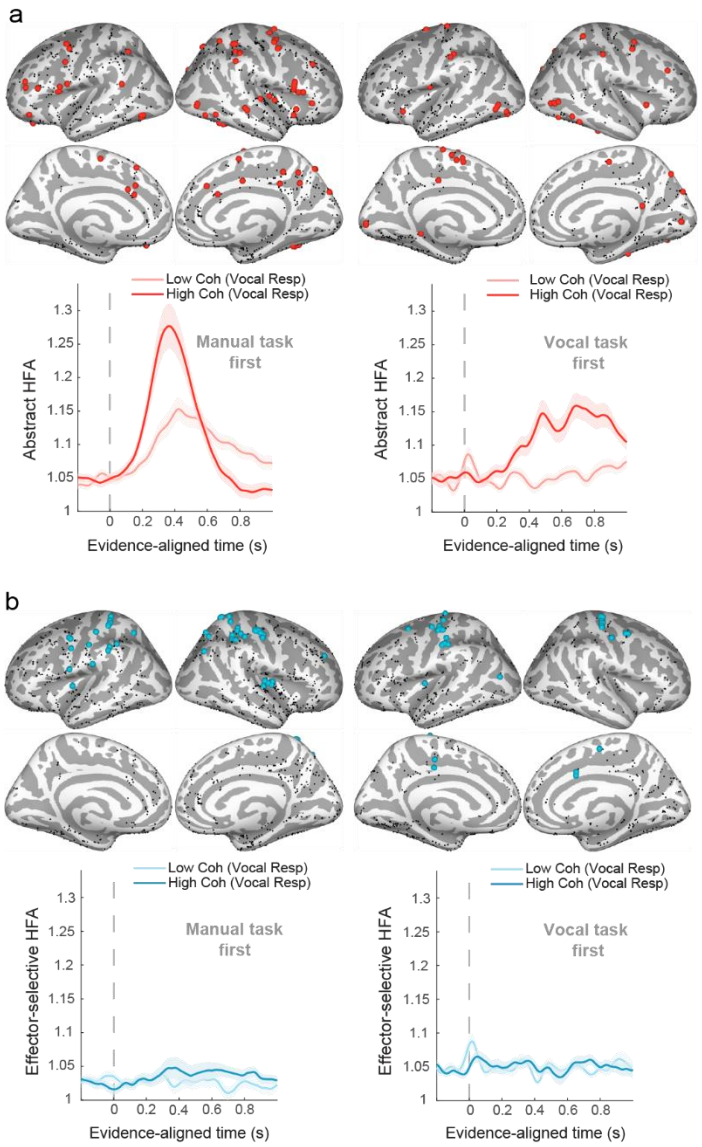

Extended Data Fig. 6. Effect of task order on activity during the vocal response task. Temporal profile of average HFA during the delayed vocal response task, in sites categorized previously (i.e. based on the manual response task) as abstract (i.e., effector independent) (**a**) vs. effector selective (**b**). Results are shown for two subject groups based on the order in which they performed the two versions of the task (*left panels*: subjects performed the manual response task first; right panel: subjects performed the vocal response first). All color conventions are the same as in Fig. 5.

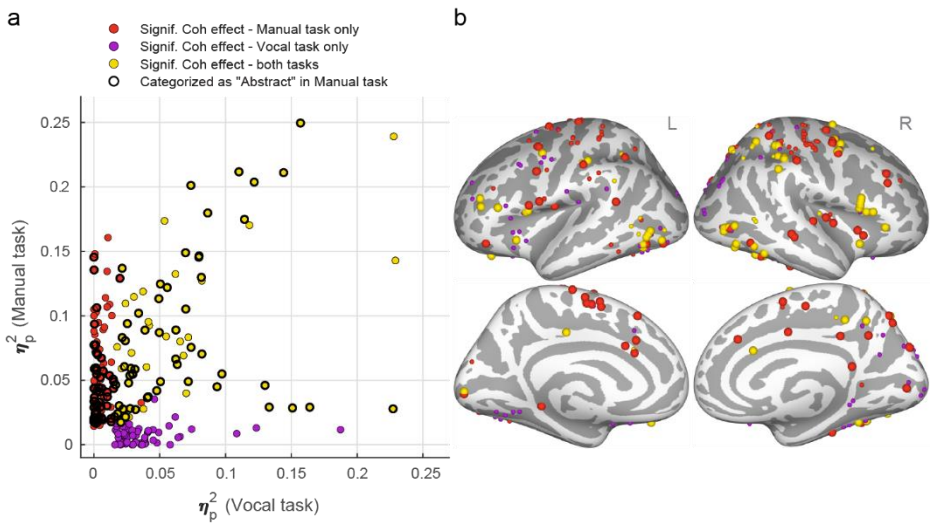

Extended Data Fig. 7. Modulation of HFA by evidence strength in contacts common between the two behavioral tasks. Displayed here are only the task-responsive contacts showing a significant effect of evidence strength (High>Low) in the evidence-aligned signal in at least one of the tasks (thresholded at p<.05, uncorrected; see ANOVA in Methods). **a.** Effect sizes (partial eta squared, η_p^2) reflecting the magnitude of the modulation by evidence strength during the vocal (*x* axis) and manual (*y* axis) response tasks. Data points represent individual contacts. **b.** Spatial distribution of evidence strength modulation (large dots: contacts categorized as abstract accumulator candidates during the manual-response task).

Data availability

Data have been made available on OSF, at: https://osf.io/9bzx8/?view_only=ed6f1eba830840cb9921458490b3c362

Code availability

Code has been made available on OSF, at: https://osf.io/9bzx8/?view_only=ed6f1eba830840cb9921458490b3c362

Acknowledgements

This work is funded by a NIH research grant to S.B., R.G.O., and S.P.K. (R01MH122513). We thank the neurology, neurosurgery, and technician teams at North Shore University and Lenox Hill hospitals for their support throughout the conduction of the study. We also thank the patients who kindly volunteered their time to participate in the research. The funders had no role in study design, data collection and analysis, decision to publish or preparation of the manuscript.

Author Contributions Statement

S.G., R.G.O, S.P.K., and S.B. designed the experiment and wrote the manuscript. S.G. recorded the neural data and performed the formal analysis. N.M., G.T., and E.E. contributed to data acquisition, preprocessing, and visualization. All authors provided feedback on data analysis and reviewed the manuscript.

Competing Interests Statement

The authors declare no competing interests.

References

1. Hanes, D. P. & Schall, J. D. Neural control of voluntary movement initiation. *Science* **274**, 427–430 (1996).
2. Kim, J. N. & Shadlen, M. N. Neural correlates of a decision in the dorsolateral prefrontal cortex of the macaque. *Nat. Neurosci.* **2**, 176–185 (1999).
3. Shadlen, M. N. & Newsome, W. T. Neural Basis of a Perceptual Decision in the Parietal Cortex (Area LIP) of the Rhesus Monkey. *J. Neurophysiol.* **86**, 1916–1936 (2001).
4. Ding, L. & Gold, J. I. Caudate Encodes Multiple Computations for Perceptual Decisions. *J. Neurosci.* **30**, 15747–15759 (2010).
5. Gold, J. I. & Shadlen, M. N. The neural basis of decision making. *Annu. Rev. Neurosci.* **30**, 535–574 (2007).
6. Lafuente, V. de, Jazayeri, M. & Shadlen, M. N. Representation of Accumulating Evidence for a Decision in Two Parietal Areas. *J. Neurosci.* **35**, 4306–4318 (2015).
7. Freedman, D. J. & Assad, J. A. Experience-dependent representation of visual categories in parietal cortex. *Nature* **443**, 85–88 (2006).
8. Bennur, S. & Gold, J. I. Distinct representations of a perceptual decision and the associated oculomotor plan in the monkey lateral intraparietal area. *J. Neurosci. Off. J. Soc. Neurosci.* **31**, 913–921 (2011).
9. Zhou, Y. & Freedman, D. J. Posterior Parietal Cortex Plays a Causal Role in Perceptual and Categorical Decisions. *Science* **365**, 180–185 (2019).
10. Zhou, Y. *et al.* Distributed functions of prefrontal and parietal cortices during sequential categorical decisions. *eLife* **10**, e58782 (2021).
11. Horwitz, G. D., Batista, A. P. & Newsome, W. T. Representation of an Abstract Perceptual Decision in Macaque Superior Colliculus. *J. Neurophysiol.* **91**, 2281–2296 (2004).
12. Heekeren, H. R., Marrett, S., Ruff, D. A., Bandettini, P. A. & Ungerleider, L. G. Involvement of human left dorsolateral prefrontal cortex in perceptual decision making is independent of response modality. *Proc. Natl. Acad. Sci.* **103**, 10023–10028 (2006).
13. Ho, T. C., Brown, S. & Serences, J. T. Domain General Mechanisms of Perceptual Decision Making in Human Cortex. *J. Neurosci.* **29**, 8675–8687 (2009).
14. Liu, T. & Pleskac, T. J. Neural correlates of evidence accumulation in a perceptual decision task. *J. Neurophysiol.* **106**, 2383–2398 (2011).
15. Hebart, M. N., Donner, T. H. & Haynes, J.-D. Human visual and parietal cortex encode visual choices independent of motor plans. *NeuroImage* **63**, 1393–1403 (2012).
16. Morito, Y. & Murata, T. Accumulation System: Distributed Neural Substrates of Perceptual Decision Making Revealed by fMRI Deconvolution. *J. Neurosci.* **42**, 4891–4912 (2022).
17. Sandhaeger, F., Omejc, N., Pape, A.-A. & Siegel, M. Abstract perceptual choice signals during action-linked decisions in the human brain. *PLOS Biol.* **21**, e3002324 (2023).
18. Wilming, N., Murphy, P. R., Meyniel, F. & Donner, T. H. Large-scale dynamics of perceptual decision information across human cortex. *Nat. Commun.* **11**, 5109 (2020).
19. Peters, M. A. K. *et al.* Perceptual confidence neglects decision-incongruent evidence in the brain. *Nat. Hum. Behav.* **1**, 0139 (2017).
20. Philiastides, M. G. & Sajda, P. Temporal characterization of the neural correlates of perceptual decision making in the human brain. *Cereb. Cortex N. Y. N 1991* **16**, 509–518 (2006).
21. Diaz, J. A., Queirazza, F. & Philiastides, M. G. Perceptual learning alters post-sensory processing in human decision-making. *Nat. Hum. Behav.* **1**, 1–9 (2017).
22. Meister, M. L. R., Hennig, J. A. & Huk, A. C. Signal multiplexing and single-neuron computations in lateral intraparietal area during decision-making. *J. Neurosci. Off. J. Soc. Neurosci.* **33**, 2254–2267 (2013).
23. O'Connell, R. G., Dockree, P. M. & Kelly, S. P. A supramodal accumulation-to-bound signal that determines perceptual decisions in humans. *Nat. Neurosci.* **15**, 1729–1735 (2012).
24. Kelly, S. P. & O'Connell, R. G. Internal and External Influences on the Rate of Sensory Evidence Accumulation in the Human Brain. *J. Neurosci.* **33**, 19434–19441 (2013).
25. Philiastides, M. G., Heekeren, H. R. & Sajda, P. Human Scalp Potentials Reflect a Mixture of Decision-Related Signals during Perceptual Choices. *J. Neurosci.* **34**, 16877–16889 (2014).
26. O'Connell, R. G. & Kelly, S. P. Neurophysiology of Human Perceptual Decision-Making. *Annu. Rev. Neurosci.* **44**, 495–516 (2021).
27. Kelly, S. P., Corbett, E. A. & O'Connell, R. G. Neurocomputational mechanisms of prior-informed perceptual decision-making in humans. *Nat. Hum. Behav.* **5**, 467–481 (2021).
28. Loughnane, G. M. *et al.* Target Selection Signals Influence Perceptual Decisions by Modulating the Onset and Rate of Evidence Accumulation. *Curr. Biol.* **26**, 496–502 (2016).
29. Twomey, D. M., Kelly, S. P. & O'Connell, R. G. Abstract and Effector-Selective Decision Signals Exhibit Qualitatively Distinct Dynamics before Delayed Perceptual Reports. *J. Neurosci. Off. J. Soc. Neurosci.* **36**, 7346–7352 (2016).

30. Steinemann, N. A., O'Connell, R. G. & Kelly, S. P. Decisions are expedited through multiple neural adjustments spanning the sensorimotor hierarchy. *Nat. Commun.* **9**, 3627 (2018).
31. Parvizi, J. & Kastner, S. Promises and limitations of human intracranial electroencephalography. *Nat. Neurosci.* **21**, 474–483 (2018).
32. Nunez, M. D., Gosai, A., Vandekerckhove, J. & Srinivasan, R. The latency of a visual evoked potential tracks the onset of decision making. *NeuroImage* **197**, 93–108 (2019).
33. Britten, K. H., Shadlen, M. N., Newsome, W. T. & Movshon, J. A. Responses of neurons in macaque MT to stochastic motion signals. *Vis. Neurosci.* **10**, 1157–1169 (1993).
34. Twomey, D. M., Murphy, P. R., Kelly, S. P. & O'Connell, R. G. The classic P300 encodes a build-to-threshold decision variable. *Eur. J. Neurosci.* **42**, 1636–1643 (2015).
35. Yeo, B. T. T. *et al.* The organization of the human cerebral cortex estimated by intrinsic functional connectivity. *J. Neurophysiol.* **106**, 1125–1165 (2011).
36. Fox, M. D., Corbetta, M., Snyder, A. Z., Vincent, J. L. & Raichle, M. E. Spontaneous neuronal activity distinguishes human dorsal and ventral attention systems. *Proc. Natl. Acad. Sci.* **103**, 10046–10051 (2006).
37. Seeley, W. W. *et al.* Dissociable Intrinsic Connectivity Networks for Salience Processing and Executive Control. *J. Neurosci.* **27**, 2349–2356 (2007).
38. Devine, C. A., Gaffney, C., Loughnane, G. M., Kelly, S. P. & O'Connell, R. G. The role of premature evidence accumulation in making difficult perceptual decisions under temporal uncertainty. *eLife* **8**, e48526 (2019).
39. Hanks, T., Kiani, R. & Shadlen, M. N. A neural mechanism of speed-accuracy tradeoff in macaque area LIP. *eLife* **3**, e02260 (2014).
40. Murphy, P. R., Boonstra, E. & Nieuwenhuis, S. Global gain modulation generates time-dependent urgency during perceptual choice in humans. *Nat. Commun.* **7**, 13526 (2016).
41. Sandhaeger, F., Omejc, N., Pape, A.-A. & Siegel, M. Abstract neural choice signals during action-linked decisions. 2020.10.02.323832 Preprint at https://doi.org/10.1101/2020.10.02.323832 (2022).
42. Tremel, J. J. & Wheeler, M. E. Content-specific evidence accumulation in inferior temporal cortex during perceptual decision-making. *NeuroImage* **109**, 35–49 (2015).
43. Pereira, M. *et al.* Evidence accumulation relates to perceptual consciousness and monitoring. *Nat. Commun.* **12**, 3261 (2021).
44. Polanía, R., Krajbich, I., Grueschow, M. & Ruff, C. C. Neural oscillations and synchronization differentially support evidence accumulation in perceptual and value-based decision making. *Neuron* **82**, 709–720 (2014).
45. Buzsáki, G., Anastassiou, C. A. & Koch, C. The origin of extracellular fields and currents--EEG, ECoG, LFP and spikes. *Nat. Rev. Neurosci.* **13**, 407–420 (2012).
46. Leszczyński, M. *et al.* Dissociation of broadband high-frequency activity and neuronal firing in the neocortex. *Sci. Adv.* **6**, eabb0977 (2020).
47. Ray, S., Crone, N. E., Niebur, E., Franaszczuk, P. J. & Hsiao, S. S. Neural Correlates of High-Gamma Oscillations (60–200 Hz) in Macaque Local Field Potentials and Their Potential Implications in Electrocorticography. *J. Neurosci.* **28**, 11526–11536 (2008).
48. Roitman, J. D. & Shadlen, M. N. Response of Neurons in the Lateral Intraparietal Area during a Combined Visual Discrimination Reaction Time Task. *J. Neurosci.* **22**, 9475–9489 (2002).
49. Thura, D. & Cisek, P. Modulation of Premotor and Primary Motor Cortical Activity during Volitional Adjustments of Speed-Accuracy Trade-Offs. *J. Neurosci. Off. J. Soc. Neurosci.* **36**, 938–956 (2016).
50. Donner, T. H., Siegel, M., Fries, P. & Engel, A. K. Buildup of choice-predictive activity in human motor cortex during perceptual decision making. *Curr. Biol. CB* **19**, 1581–1585 (2009).
51. Selimbeyoglu, A. & Parvizi, J. Electrical stimulation of the human brain: perceptual and behavioral phenomena reported in the old and new literature. *Front. Hum. Neurosci.* **4**, 46 (2010).
52. Ding, L. & Gold, J. I. The basal ganglia's contributions to perceptual decision-making. *Neuron* **79**, 640–649 (2013).
53. Yartsev, M. M., Hanks, T. D., Yoon, A. M. & Brody, C. D. Causal contribution and dynamical encoding in the striatum during evidence accumulation. *eLife* **7**, e34929 (2018).
54. Groppe, D. M. *et al.* iELVis: An open source MATLAB toolbox for localizing and visualizing human intracranial electrode data. *J. Neurosci. Methods* **281**, 40–48 (2017).
55. Smith, S. M. Fast robust automated brain extraction. *Hum. Brain Mapp.* **17**, 143–155 (2002).
56. Jenkinson, M. & Smith, S. A global optimisation method for robust affine registration of brain images. *Med. Image Anal.* **5**, 143–156 (2001).
57. Jenkinson, M., Bannister, P., Brady, M. & Smith, S. Improved optimization for the robust and accurate linear registration and motion correction of brain images. *NeuroImage* **17**, 825–841 (2002).
58. Papademetris, X. *et al.* BioImage Suite: An integrated medical image analysis suite: An update. *Insight J.* **2006**, 209 (2006).
59. Fischl, B. FreeSurfer. *NeuroImage* **62**, 774–781 (2012).
60. Mercier, M. R. *et al.* Evaluation of cortical local field potential diffusion in stereotactic electro-encephalography recordings:

A glimpse on white matter signal. *NeuroImage* **147**, 219–232 (2017).
61. Shadlen, M. N. & Kiani, R. Decision making as a window on cognition. *Neuron* **80**, 791–806 (2013).
62. Aarts, E., Verhage, M., Veenvliet, J. V., Dolan, C. V. & van der Sluis, S. A solution to dependency: using multilevel analysis to accommodate nested data. *Nat. Neurosci.* **17**, 491–496 (2014).
63. Desikan, R. S. *et al.* An automated labeling system for subdividing the human cerebral cortex on MRI scans into gyral based regions of interest. *NeuroImage* **31**, 968–980 (2006).